Università degli Studi di Bari Aldo Moro

FACOLTÀ DI SCIENZE MATEMATICHE, FISICHE E NATURALI

CORSO DI LAUREA MAGISTRALE IN FISICA

titolo

Relatore:
Dott.ssa Anna Colaleo

Laureando:
Filippo Errico

ANNO ACCADEMICO 2013-2014

Contents

Chapter 1

The CMS detector at LHC

1.1 The Large Hadron Collider

Approved in the early '90s and started up in the 2008, the *Large Hadron Collider* (LHC) is currently the world's largest and most powerful particle accelerator.
Its main purpose is to help in testing the predictions of different theories of particle physics.
LHC [16], situated at the CERN laboratories of Geneva, is a proton-proton (pp) collider built to work at the design center of mass energy of $\sqrt{s} = 14$ TeV, with a bunch crossing every 25 ns and a design luminosity of 10^{34} cm^{-2} s^{-1}. It is installed in the same circular underground tunnel occupied until the year 2000 by the Large Electron Positron collider (LEP). The pp collision are used, instead of the e^+e^- one of LEP, to reduce the synchrotron radiation, in order to accelerate the particles up to a very large energy. It was preferred to a $p\bar{p}$ collider because it allows to reach higher rate of events. In fact the low anti-proton production efficiency (10^5 protons are needed to create an anti-proton) and larger time needed to accumulate them, would make almost impossible to reach the high design luminosity of the LHC. The luminosity L is the parameter to quantify the performances of a collider, because the event rate R_i of a given process i, defined as the number of events occurring per unit of time, can be written as:

$$R_i = \frac{dN_i}{dt} = L \cdot \sigma_i \tag{1.1}$$

where σ_i is the cross section of the process i. The luminosity depends only on the machine parameters. Assuming a small crossing angle between the beams and Gaussian-shaped beam bunches, the luminosity L can be written as:

$$L = \frac{f n_b N^2}{4\pi\sigma^2} \tag{1.2}$$

where f is the revolution frequency of particle bunches, n_b is the number of bunches rotating in the accelerator, N is the number of protons in the two colliding bunches and σ is the RMS of beam profile distributions in the plane orthogonal to the beam direction.

In the LHC design, 1232 main dipole magnets (made of niobium-titanium super-conductor chilled with superfluid Helium at 1.9 K) generating a magnetic field up to 8.3 T, will be used to steer the particles into curvilinear trajectories. The two beams will run in two contiguous pipes with vacuum inside, separated by 19.4 cm, that will be unified in proximity of the interactions points, where the experiments will be placed. Because of the high luminosity of the LHC, large thermal power will be generated near the pipes due to the synchrotron radiation, making necessary the presence of a suitable cooling system. For this reason also the pipes will be in contact with superfluid Helium at 1.9 K.
In Figure 1.1 is shown the complete scheme of the accelerator chain of the LHC: the proton beam is created by using an electric field to pull the electrons from hydrogen atoms and start the acceleration. Protons are injected into the PS Booster (PSB) at an energy of 50 MeV from Linac2 (Linear Accelerator 2). The booster comprises four superposed rings: this is because at low energy intensity, the quality of the beams suffers from the repulsive forces between particles. By splitting up the injected beam this effect gets reduced. Once the beam reaches the energy of 1.4 GeV it is extracted and injected into Proton Synchrotron (PS). With a circumference of 628 m, the PS accelerates the beams up to 26 GeV when they are extracted and sent to the Super Proton Synchrotron (SPS). Built in the '70, the SPS has a length of 7 km. The beam is injected at 26 GeV, ramped up to 450 GeV and extracted to the LHC.
Once the energy-working point is reached, the beams are made to collide at four loca-

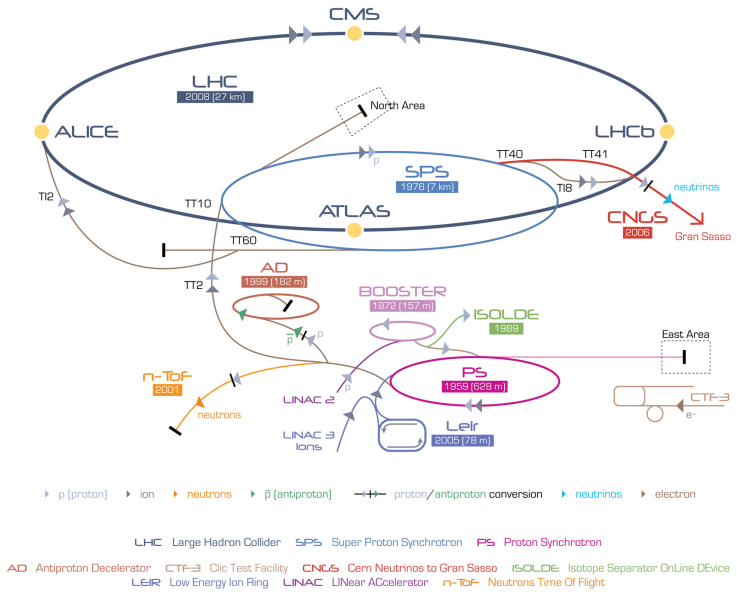

Figure 1.1: Accelerator scheme at CERN.

tions around the LHC, corresponding to the position of four particles detectors: ALICE (*A Large Ion Collider Experiment*), ATLAS (*A Toroidal LHC ApparatuS*), CMS (*Compact Muon Solenoid*) and LHCb (*Large Hadron Collider beauty*). In addition to these,

there are other three experiment installed at the LHC: TOTEM (*TOTal Elastic and diffractive cross section Measurement*) installed close to CMS, MoEDAL (*Monopole and Exotics Detector at the LHC*) close to LHCb and LHCf (*Large Hadron Collider forward*) near ATLAS.
The beams at LHC have a bunch structure as a direct consequence of the radio frequency acceleration scheme. Protons can only be accelerated when the RF field has the correct orientation when particles pass through an accelerating cavity. Under nominal operating conditions, each proton beam has 2808 bunches, with each bunch containing about 10^{11} protons. The bunch size is not constant around the ring getting squeezed as much as possibile around the interaction points in order to increase the probability of collision. They measure a few centimetres long and a millimetre wide when they are far from a collision point; as the bunches approach the collision points, they are squeezed to about 20 μm. LHC uses a bunch spacing of 25 ns (or 7.5 m) corresponding to a frequency of 40 MHz.
In Table 1.1 are reported the designed LHC parameters and the ones reached at the end of RunII in 2018.

		Design	2018
Centre of mass energy	E	14 TeV	13 TeV
Luminosity	L	10^{34} cm^{-2}s^{-1}	—
Time spacing		25 ns	25 ns
Num. of bunches	k_B	2808	—
Num. protons per bunch	N_p	1.15×10^{11}	—

Table 1.1: LHC parameters

1.2 The Compact Muon Solenoid

The Compact Muon Solenoid (CMS) is one of the general purpose experiments which takes data at the LHC. Its physics goals range from the search for the Higgs boson to the searches for physics beyond the Standard Model, to the precision measurements of already known particles and phenomena [17].
The overall layout of CMS is shown in Figure 1.2. The inner tracker and the two calorimeters of CMS are located inside a 13 m-long, 5.9 m inner diameter, 3.8 T superconducting solenoid. In order to achieve good momentum resolution within a compact spectrometer without making stringent demands on muon-chamber resolution and alignment, a high magnetic field was chosen. The return field is large enough to saturate 1.5 m of iron, allowing four muon stations to be integrated to ensure robustness and full geometric coverage. The central part of CMS is called *barrel* while the two edges of the detector are denoted as *endcaps*. The tracking volume is given by a cylinder of length 5.8 m and diameter 2.6 m. In order to deal with high track multiplicities, CMS employs 10 layers

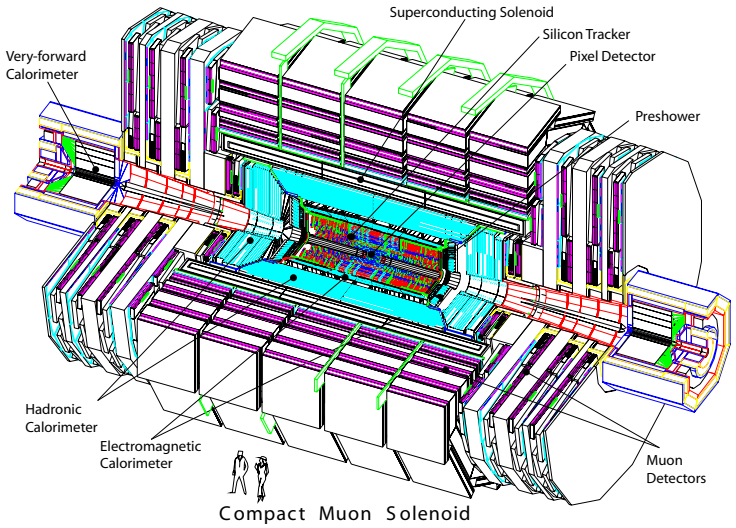

Figure 1.2: CMS detector overview.

of silicon microstrip detectors, which provide the required granularity and precision. In addition, 3 layers of silicon pixel detectors are placed close to the interaction region to improve the measurement of the impact parameter of charged-particle tracks, as well as the position of secondary vertexes. The electromagnetic calorimeter (ECAL) uses lead tungstate ($PbWO_4$) crystals with coverage in pseudorapidity up to $|\eta| < 3.0$. A preshower system is installed in front of the edges of ECAL for π^0 rejection.

Coordinate Conventions

The coordinate system adopted by CMS has the origin centered at the nominal collision point inside the experiment, the y-axis pointing vertically upward, and the x-axis pointing radially inward toward the center of the LHC. Thus, the z-axis points along the beam direction toward the Jura mountains from LHC Point 5. The azimuthal angle ϕ is measured from the x-axis in the x-y plane. The polar angle θ is measured from the z-axis. Pseudorapidity is defined as

$$\eta = -\ln\tan(\theta/2) \tag{1.3}$$

The value $\eta = 0$ corresponds to a direction perpendicular to the beamline, while the limit $\eta = \infty$ gives a direction parallel to the beamline. The momentum and energy measured transverse to the beam direction, denoted by p_T and E_T, respectively, are computed as follow:

$$p_T = psin\theta \tag{1.4}$$

$$E_T = Esin\theta \tag{1.5}$$

Finally, particles which escape the detection leave an imbalance in the transverse plane which is quantified as missing transverse energy in the following way:

$$E_T^{miss} = -\sum_i p_T^i \tag{1.6}$$

as the negative vectorial sum of the transverse momentum of all the visible particles in the event.

1.2.1 The tracking system

The tracker [18, 19] , placed within the magnetic field, is the subdetector which is closer to the interaction point. It is dedicated to track and vertex finding. The silicon (Si) technology has been chosen for the whole tracker in order to provide good radiation hardness, high granularity and large hit redundancy to perform a good pattern recognition. The layout of the CMS tracker is shown in Figure 1.3. Close to the interaction vertex, in the barrel region, are 3 layers of hybrid pixel detectors at a radius (r) of about 4, 7 and 10 cm. The size of the pixel detector is $100 - 150$ m^2. In the barrel part, the Si microstrip detectors are placed at r between 20 and 110 cm. The forward region has 2 pixel and 9 microstrip layers in each of the two endcaps. In order to avoid excessively shallow track crossing angles, the Inner Barrel is shorter than the Outer Barrel, and there are additional three Inner Disks in the transition region between barrel and endcaps, on each side of the Inner Barrel. The total area of the Si detectors is around 200 m^2, providing a coverage up to $\eta = 2.5$. The material budget inside the active volume of the tracker increases from 0.4 radiation length (X_0) at $\eta = 0$ to around 1 X_0 at $|\eta| = 1.6$, before decreasing to 0.6 X_0 at $|\eta| = 2.5$.

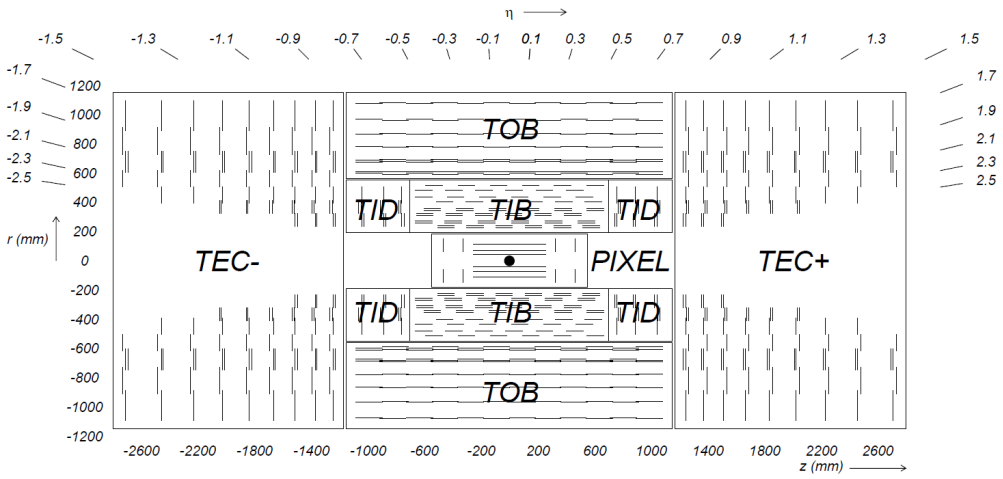

Figure 1.3: Schematic cross section through the CMS tracker in the $r - z$ plane: each line represents a detector module. Double lines indicate back-to-back modules which deliver stereo hits.

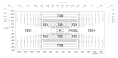

Figure 1.4: Material budget in units of radiation length as a function of pseudorapidity η for the different sub-detectors (left panel) and broken down into the functional contributions (right panel).

The pixel detector

The pixel system is the part of the tracking system that is closest to the interaction region and covers a pseudorapidity range $-2.5 < \eta < 2.5$, matching the acceptance of the central tracker. Figure 1.5 shows the geometric pixel strcture. It contributes precise tracking points in $r-\phi$ and z and therefore is responsible for a small impact parameter resolution that is important for good secondary vertex reconstruction. With a pixel cell size of 100×150 μm^2 emphasis has been put on achieving similar track resolution in both $r-\phi$ and z directions: 10 μm in $r-\phi$ direction and 20 μm along z. The pixel detector is essential for the reconstruction of secondary vertices from b and tau decays, and forming seed tracks for the outer track reconstruction and high level triggering. It consists of three barrel layers (BPix) with two endcap disks (FPix). The 53-cm-long BPix layers will be located at mean radii of 4.4, 7.3 and 10.2 cm. The FPix disks, extending from $\approx$ 6 to 15 cm in radius, will be placed on each side at z=$\pm$34.5 and z=$\pm$46.5 cm. BPix (FPix) contain 48 million (18 million) pixels covering a total area of 0.78 (0.28) m^2. The arrangement of the 3 barrel layers and the forward pixel disks on each side gives 3 tracking points over almost the full η range. In the high η region the 2 disk points are combined with the lowest possible radius point from the 4.4 cm barrel layer.

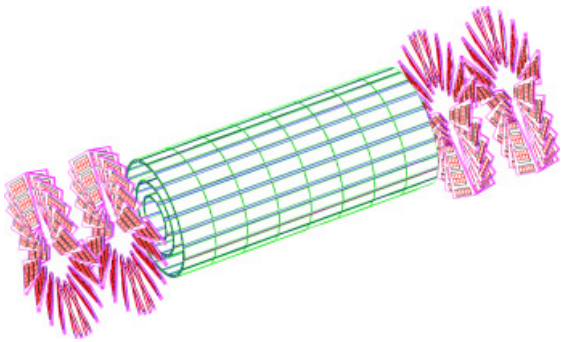

Figure 1.5: Geometrical layout of the pixel detector.

Pixel Upgrade

Due to the radiation damage and significant data losses due to high occupancy in the readout chip of the pixel detector, the pixel system has been replaced by a new one in the end-of-year shutdown during winter 2016/2017 in order to maintain the excellent

tracking and other physics performances [20]. The main new features of the upgraded pixel detector are a ultra-light mechanical design with four barrel layers and three end-cap disks, digital readout chip with higher rate capability and a new cooling system. The geometrical layout of the upgrade system, shown in Figure 1.6, consists of four

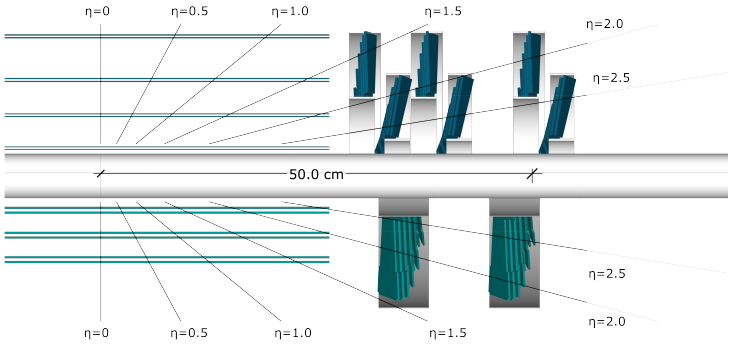

Figure 1.6: Comparison of the geometrical layouts of the old (bottom) and upgraded (top) CMS pixel detectors.

cylindrical barrel layers placed at radii of 29, 68, 109, 160 mm and three disks in each of the forward regions placed at a distance from the nominal interaction point of 291, 396 and 516 mm. This layout is optimized in order to offer full 4-hit tracking coverage up to pseudorapidities of 2.5, with an increased redundancy compared to the present system.

The silicon strip detector

The silicon strip detector is composed of three different subsystem. The Tracker Inner Barrel and Disks (TIB/TID see Figure 1.3) are composed of 4 barrel layers, supplemented by 3 disks at each end. TIB/TID delivers up to 4 $r-\phi$ measurements on a trajectory using 320 μm thick silicon microstrip sensors with their strips parallel to the beam axis in the barrel and radial on the disks. The strip pitch is 80μm on layers 1 and 2 and 120 μm on layers 3 and 4 in the TIB, leading to a single point resolution of 23 μm and 35 μm, respectively. In the TID the mean pitch varies between 100μm and 141μm. The TIB/TID is surrounded by the Tracker Outer Barrel (TOB). It has an outer radius of 116 cm and consists of 6 barrel layers of 500μm thick microstrip sensors with strip pitches of 183μm on the first 4 layers and 122μm on layers 5 and 6. It provides another 6 $r-\phi$ measurements with single point resolution of 53μm and 35μm, respectively. The TOB extends in z between ±118cm. Beyond this z range the Tracker EndCaps (±TEC, where the sign indicates the location along the z axis) cover the region 124 cm $< |z| <$ 282 cm and 22.5 cm $< |r| <$113.5 cm. Each TEC is composed of 9 disks, carrying up to 7 rings of silicon microstrip detectors (320μm thick on the inner 4 rings, 500μm thick on rings 5-7) with radial strips of 97μm to 184μm average pitch. Thus, they provide up to 9 ϕ measurements per trajectory. In addition, the modules in the first two layers and

rings, respectively, of TIB, TID, and TOB as well as rings 1, 2, and 5 of the TECs carry a second microstrip detector module which is mounted back-to-back with a stereo angle of 100 mrad in order to provide a measurement of the second coordinate (z in the barrel and r on the disks). The achieved single point resolution of this measurement is $230\mu m$ and $530\mu m$ in TIB and TOB, respectively, and varies with pitch in TID and TEC.
The sensor elements in the strip tracker are single sided p-on-n type silicon micro-strip sensors shown in Figure 1.7: in TIB/TID and on the inner 4 rings of the TECs, thin sensors of (320 $\pm$ 20) μm wafer thickness are used, with substrate resistivity of ro = 1.55 - 3.25 kΩcm; TOB and the outer 3 rings of the TECs are equipped with thicker sensors of (500 $\pm$ 20) μm thickness, with substrate resistivity of ro = 4 - 8 kΩcm.

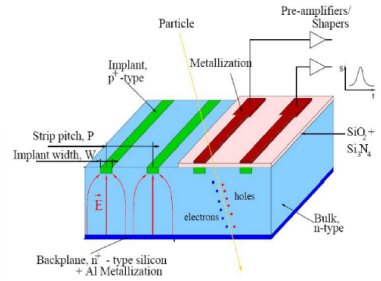

Figure 1.7: Single sided p-on-n type silicon micro-strip sensor.

LASER ALIGNMENT SYSTEM

1.2.2 Electromagnetic calorimeter

The electromagnetic calorimeter plays an essential role in the study of the physics of electroweak symmetry breaking, and in the exploration of beyond the Standard Model scenarios. ECAL is a homogeneous calorimeter of almost 76000 Lead Tungstate $PbWO_4$ scintillating crystals divided into a barrel and two endcaps. A 3D view of the barrel and endcap electromagnetic calorimeter is shown in Figure 1.8.

The Barrel Calorimeter

The barrel part of the ECAL covers the pseudorapidity range $|\eta| < 1.479$ The front face of the crystals is at a radius of 1.29 m and each crystal has a square cross-section of $22 \times 22\,\mathrm{mm}^2$ and a length of 230 mm corresponding to $25.8\,\mathrm{X}_0$. The truncated pyramid-shaped crystals are mounted in a geometry which is off-pointing with respect to the mean position of the primary interaction vertex, with a 3° tilt in both ϕ and in η. The crystal cross-section corresponds to $\Delta\eta \times \Delta\phi = 0.0175 \times 0.0175$ (1°). The barrel granularity is 360-fold in ϕ and (2×85)-fold in η, resulting in a total number of 61 200 crystals. The crystal volume in the barrel amounts to $8.14\,\mathrm{m}^3$ (67.4 t). Crystals for each half-barrel are grouped in 18 supermodules each subtending 20° in ϕ. Each supermodule comprises four modules with 500 crystals in the first module and 400 crystals in each of the remaining three modules. For simplicity of construction and assembly, crystals have

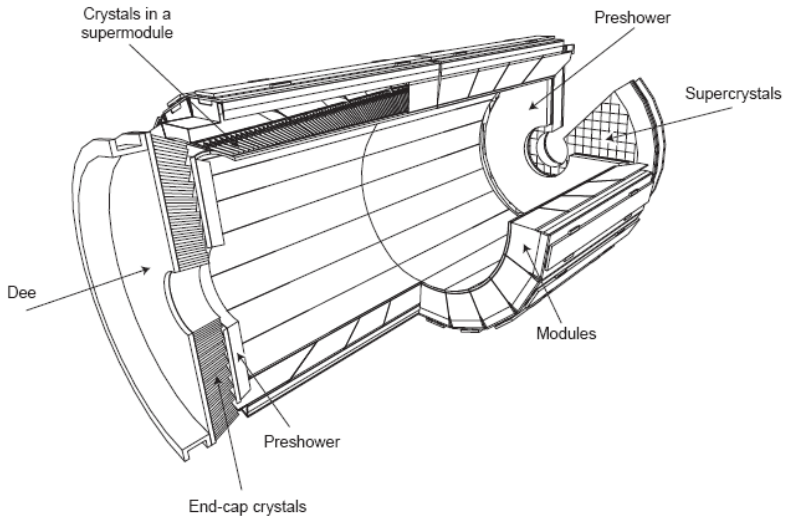

Figure 1.8: A 3D view of the electromagnetic calorimeter.

been grouped in arrays of 2×5 crystals which are contained in a very thin wall ($200\,\mu$m) alveolar structure and form a submodule. Thermal regulation is carried out by two active systems: 1) a specially regulated cooling circuit which keeps the operating temperature (ambient temperature) of the crystal array and of the APDs within a tight temperature spread of $\pm 0.05\,^{\circ}$C, ensuring adequate thermal stability; 2) the power cooling circuit evacuates the heat generated by all power sources in the supermodule (each supermodule is designed as a separate thermal entity).

Bibliography

[1] C. Patrignani et al. (Particle Data Group), Chin. Phys. C, 40, 100001 (2016) and 2017 update.

[2] Halzen and Martin, *Quarks and Leptons: An Introductory Course in Modern Particle Physics*, John Wiley & Sons (1984).

[3] M.E.Peskin and D.V.Schroeder, *An Introduction To Quantum Field Theory*, Addison-Wesley, 1995.

[4] M.Maggiore, *A Modern Introduction to Quantum Filed Theory*, Oxford University Press, 2004.

[5] A.Pich, *The standard model of electroweak interactions*, arXiv:hep-ph/0502010v, 2005.

[6] UA1 Collaboration, *Experimental observation of isolated large transverse energy electrons with associated missing energy at sqrts* $= 540\ GeV$.

[7] UA1 Collaboration, *Experimental observation of lepton pairs of invariant mass around* $95\ GeV/c^2$ *at the CERN SPS collider.*

[8] S. Weinberg, *A model of leptons*, Phys. Rev. Lett. 19 (1967) 1264.

[9] MuLan Collaboration, *Improved Measurement of the Positive Muon Lifetime and Determination of the Fermi Constant*, Phys.Rev.Lett.99:032001,2007, arXiv:0704.1981.

[10] ATLAS Collaboration, *Observation of a new particle in the search for the Standard Model Higgs boson with the ATLAS detector at the LHC*, Phys.Lett. B716 (2012), pp. 1-29, DOI: 10.1016/j.physletb.2012.08.020.

[11] CMS Collaboration, *Observation of a new boson at a mass of 125 GeV with the CMS experiment at the LHC*, Physics Letters B716 (2012), pp. 30-61. DOI: http://dx.DOI.org/10.1016/j.physletb.2012.08.021 .

[12] LHC Higgs Cross Section Working Group, https://twiki.cern.ch/twiki/bin/view/LHCPhysics/LHCHXSWG.

[13] D. de Florian et al., [LHC Higgs Cross Section Working Group], CERN-2017-002-M, arXiv:1610.07922[hep-ph] (2016).

[14] S. Heinemeyer et al., [LHC Higgs Cross Section Working Group], CERN?2013?004, arXiv:1307.1347 [hep-ph] (2013).

[15] D. de Florian et al., [LHC Higgs Cross Section Working Group], CERN?2017?002-M, arXiv:1610.07922[hep-ph] (2016).

[16] Lyndon Evans and Philip Bryant, [LHC Machine], 1748-0221-3-08-S08001, Journal of Instrumentation (2008), http://stacks.iop.org/1748-0221/3/i=08/a=S08001

[17] CMS collaboration, [The Compact Muon Solenoid technical proposal], CERN-LHCC-94-38, http://cdsweb.cern.ch/record/290969

[18] CMS collaboration, [The CMS tracker system project: technical design report], CERN-LHCC-98-006, http://cdsweb.cern.ch/record/368412.

[19] CMS collaboration, [The CMS tracker: addendum to the technical design report] CERN-LHCC-2000-016, http://cdsweb.cern.ch/record/490194.

[20] Anirban Saha, [Phase 1 upgrade of the CMS pixel detector], Journal of Instrumentation (2017), http://stacks.iop.org/1748-0221/12/i=02

[21] PARTICLE DATA GROUP collaboration, S. Eidelman et al., [Review of particle physics] Phys. Lett. B 592 (2004) 1.